THE JOURNAL OF PHYSICAL CHEMISTRY LETTERS
A JOURNAL OF THE AMERICAN CHEMICAL SOCIETY

pubs.acs.org/JPCL Letter

Quantum Simulations of Vibrational Strong Coupling via Path Integrals

Tao E. Li,* Abraham Nitzan, Sharon Hammes-Schiffer, and Joseph E. Subotnik

Cite This: *J. Phys. Chem. Lett.* 2022, 13, 3890−3895 Read Online

ACCESS | Metrics & More | Article Recommendations | Supporting Information

ABSTRACT: A quantum simulation of vibrational strong coupling (VSC) in the collective regime via thermostated ring-polymer molecular dynamics (TRPMD) is reported. For a collection of liquid-phase water molecules resonantly coupled to a single lossless cavity mode, the simulation shows that as compared with a fully classical calculation, the inclusion of nuclear and photonic quantum effects does not lead to a change in the Rabi splitting but does broaden polaritonic line widths roughly by a factor of 2. Moreover, under thermal equilibrium, both quantum and classical simulations predict that the static dielectric constant of liquid water is largely unchanged inside vs outside the cavity. This result disagrees with a recent experiment demonstrating that the static dielectric constant of liquid water can be resonantly enhanced under VSC, suggesting either limitations of our approach or perhaps other experimental factors that have not yet been explored.

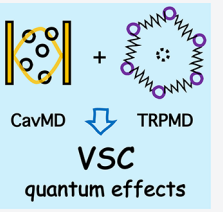

In the presence of strong light−matter interactions, molecular properties can be modified by forming hybrid light−matter states, known as polaritons.[1−8] Recently, a great deal of interest has been focused on the vibrational strong coupling (VSC) regime,[9,10] in which the bright collective mode of molecular vibrations forms a pair of upper and lower polaritons (UP and LP) with an optical cavity mode in a Fabry−Pérot microcavity. Experiments have shown that forming VSC can resonantly modify ground-state chemical reaction rates,[11−17] crystallization processes,[18] and supramolecular assembly,[19] although some of these experimental studies have not yet been reproduced.[20,21]

The experiments above represent intriguing breakthroughs in the field of chemistry. A theoretical understanding of VSC,[22−29] however, is still lacking. Although simple model systems with analytical solutions often provide useful insights about experiments, in some cases numerical simulations of realistic molecules inside the cavity[26,29−31] are necessary to explain experimental observations under VSC. Along this direction, we have developed a classical cavity molecular dynamics (CavMD) scheme.[31] This approach self-consistently propagates the coupled classical dynamics between a few cavity modes and a large ensemble of condensed-phase molecules moving on an electronic ground-state surface. Equipped with this approach, we have carefully scrutinized some fundamental VSC processes and gained understanding about existing[31−34] and potentially interesting[35] experiments. However, one outstanding question remains: to what extent can we trust *classical* simulations? Because the molecular vibrational frequencies and cavity frequencies involved in VSC are usually much larger than room temperature (300 K ∼ 209 cm^{-1}), quantum effects cannot be simply ignored.

Here, to investigate the potential impact of nuclear and photonic quantum effects, we report the first quantum CavMD simulation of liquid water under VSC by path-integral techniques.[36−39] While path-integral techniques have been used to study strong light−matter interactions,[24,40,41] a realistic simulation in the collective regime has not yet been reported. Because of the importance of liquid water, understanding how nuclear and photonic quantum effects alter the VSC dynamics[17,20,42−44] is fundamentally intriguing. Apart from this fundamental motivation, performing a quantum simulation is also needed for a better understanding of the gap between recent VSC experiments and theory. For example, a recent VSC experiment in liquid water[44] shows that under thermal equilibrium proton conductivity and the static dielectric constant of liquid water can be resonantly enhanced under VSC. At the same time, however, our previous analytical studies[24] and classical CavMD simulations[31] have demonstrated that all equilibrium properties of liquid water should be practically the same in and out of the cavity. Given that the static dielectric constant is also an equilibrium property,[45] there is clearly an inconsistency between our previous classical simulations and experiments. Hence, a quantum simulation becomes necessary to better understand this conflict. Moreover, because a hypothetical resonant effect for the dielectric constant would be similar to resonant effects in VSC catalytic experiments,[11−17] understanding whether or how VSC induces a resonant enhancement of the static dielectric constant may be very important for interpreting VSC catalytic experiments.

Before demonstrating the results, we briefly outline the fundamentals of path-integral techniques and CavMD. Path-

Received: February 28, 2022
Accepted: April 21, 2022

https://doi.org/10.1021/acs.jpclett.2c00613
J. Phys. Chem. Lett. 2022, 13, 3890−3895

integral molecular dynamics (PIMD) can accurately calculate quantum equilibrium properties of distinguishable particles at finite temperatures,[46] for which nuclei of molecules moving in an electronic ground state are a good approximation. Ring-polymer molecular dynamics (RPMD)[37−39] extends PIMD and can also approximate quantum dynamical properties of molecules reasonably well, especially for condensed-phase systems at finite temperatures, where dephasing processes can easily destroy quantum entanglement and make the molecular system more "classical". In PIMD and RPMD, quantum dynamics of molecules are propagated in an extended classical phase space, in which P classical beads interact with each other through a harmonic interbead interaction. Because of this interbead interaction, nuclear quantum effects, including zero-point energy,[47] delocalization, and quantum tunneling, can be efficiently described. However, because of spurious resonances among the normal modes of the beads, RPMD can sometimes fail to accurately describe the molecular spectrum in the high-frequency domain.[48] One simple means to solve this issue is to perform thermostated RPMD (TRPMD),[49,50] in which higher frequency internal modes of the ring polymer are attached to an additional thermostat. For our simulations, because the Rabi splitting in the high-frequency domain is critical for VSC, we will perform TRPMD instead of the standard RPMD. A more detailed description of RPMD is also given in section I of the Supporting Information.

After introducing TRPMD, let us briefly review the fundamentals of CavMD. Within the framework of CavMD, the quantum electrodynamical (QED) Hamiltonian on the electronic ground state is[24,31,51]

$$\hat{H}^{\mathrm{G}}_{\mathrm{QED}} = \hat{H}^{\mathrm{G}}_{\mathrm{M}} + \hat{H}^{\mathrm{G}}_{\mathrm{F}} \tag{1a}$$

where $\hat{H}^{\mathrm{G}}_{\mathrm{M}}$ denotes the standard (kinetic + potential) molecular Hamiltonian, and the field-related Hamiltonian $\hat{H}^{\mathrm{G}}_{\mathrm{F}}$ is

$$\hat{H}^{\mathrm{G}}_{\mathrm{F}} = \sum_{k,\lambda} \frac{\hat{\tilde{p}}_{k,\lambda}^{\,2}}{2m_{k,\lambda}} + \frac{1}{2} m_{k,\lambda}\omega_{k,\lambda}^{\,2}\left(\hat{\tilde{q}}_{k,\lambda} + \frac{\hat{d}_{g,\lambda}}{\omega_{k,\lambda}\sqrt{\Omega\epsilon_0 m_{k,\lambda}}}\right)^2 \tag{1b}$$

Here, $\hat{\tilde{p}}_{k,\lambda}$, $\hat{\tilde{q}}_{k,\lambda}$, $\omega_{k,\lambda}$, and $m_{k,\lambda}$ denote the momentum operator, position operator, frequency, and auxiliary mass for each cavity photon mode with wave vector $\mathbf{k}$ ($k = |\mathbf{k}|$) and polarization direction defined by a unit vector $\boldsymbol{\xi}_\lambda$ (with $\boldsymbol{\xi}_\lambda \cdot \mathbf{k} = 0$). $\hat{d}_{g,\lambda}$ denotes the ground-state molecular dipole operator of the whole molecular subsystem projected along the polarization direction $\boldsymbol{\xi}_\lambda$. In many cases, $\hat{d}_{g,\lambda} = \sum_{n=1}^{N} \hat{d}_{ng,\lambda}$ can be expressed as a summation of the dipole operators of each individual molecule, where N denotes the total molecular number. Ω denotes the cavity volume, and ϵ_0 denotes the vacuum permittivity. Although eq 1b has a summation over many cavity modes, in practice, during simulations, we will take into account only one cavity mode (with two polarization directions) that is at resonance with the molecular vibrational mode.

Clearly, in the QED Hamiltonian defined by eq 1, the cavity photons can be regarded as additional "nuclear" degrees of freedom of the molecular system, and the interaction potential between cavity photons and molecules (the last term in eq 1b) depends on the position operators only. In other words, eq 1 resembles a standard (kinetic + potential) molecular Hamiltonian, so we can directly apply TRPMD to calculate quantum equilibrium and dynamical properties of both the molecules and the cavity photons in the same manner as TRPMD for the molecules outside the cavity. In our implementation, the nuclei and cavity photons are each represented by 32 beads (P = 32). To distinguish between these simulations and TRPMD simulations outside the cavity, we will often refer to our generalized TRPMD simulations under VSC as quantum CavMD simulations. Note that when the number of beads becomes unity (P = 1), the quantum CavMD approach is reduced to classical CavMD.

For our simulation of liquid water under VSC, the molecular system is described with the empirical force field q-TIP4P/F.[52] This force field is commonly used in the path-integral community and can roughly generate experimentally comparable nonreactive properties of liquid water, including IR spectroscopy, the diffusion constant, and the static dielectric constant.[52,53] The liquid water system is represented by 216 H_2O molecules in a cubic simulation cell under periodic boundary conditions at 300 K. Inside the cavity, this molecular system is coupled to a lossless cavity mode (with two possible polarization directions x and y), and the effective coupling strength between each molecule and the cavity mode is set as $\tilde{\epsilon} = 4 \times 10^{-4}$ au. See section II of the Supporting Information for a more detailed explanation of the definition of $\tilde{\epsilon}$ and why our simulation can be interpreted as corresponding to Fabry−Pérot experiments. Other simulation details are explained in section III of the Supporting Information. As far as the technical details are concerned, CavMD is implemented by modifying the I-PI package,[54] the nuclear forces are evaluated by LAMMPS,[55] and the raw simulation data are available at Github.[56]

We first report the linear IR spectrum of liquid water by Fourier transforming the dipole autocorrelation function from equilibrium CavMD simulations.[31,52] Outside the cavity, as shown in Figure 1a, the classical IR spectrum (black line)

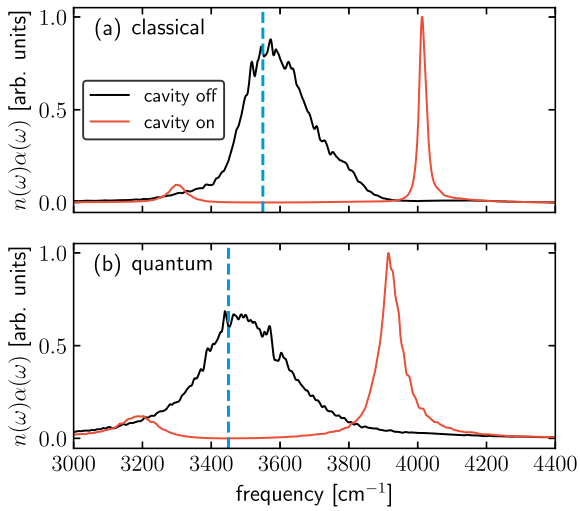

Figure 1. IR absorption spectra of liquid water from (a) classical and (b) quantum simulations. In each panel, a pair of polaritons (red line) form when the O−H stretch band (black line) is nearly resonantly coupled to the cavity mode with ω_c = 3550 cm^{-1} (classical) or 3450 cm^{-1} (quantum), as indicated by the vertical dashed blue line, with $\tilde{\epsilon} = 4 \times 10^{-4}$ au. Upon comparison of the quantum results to the classical results, the Rabi splitting remains unchanged, but the polariton line widths are significantly broadened by roughly a factor of 2; see Table 1 for the exact values.

https://doi.org/10.1021/acs.jpclett.2c00613
J. Phys. Chem. Lett. 2022, 13, 3890−3895

shows a broad band peaking near ω_0 = 3550 cm^{-1}, which corresponds to the O−H stretch modes of liquid water. The full width at half-maximum (FWHM) of this O−H stretch band is γ_{OH} = 215 cm^{-1}. Such a large line width arises from inhomogeneous broadening due mainly to the static disorder of liquid water. However, the classical O−H line width is still considerably smaller than the experimental value of nearly 400 cm^{-1}.[57] Inside the cavity, when the O−H stretch band is resonantly coupled to a lossless cavity mode with frequency ω_c = 3550 cm^{-1} (the vertical dashed blue line) and an effective coupling strength $\tilde{\varepsilon} = 4 \times 10^{-4}$ au, a pair of asymmetric UP and LP forms with a Rabi splitting of Ω_R = 715 cm^{-1}. Although the usual definition of ultrastrong coupling is $\Omega_R/2\omega_0 > 0.1$,[5] our value of Rabi splitting sits at the boundary between strong and ultrastrong coupling, so we will refer to our case as strong coupling only. The line widths of the UP and LP are γ_{UP} = 24 cm^{-1} and γ_{LP} = 60 cm^{-1}, respectively. Clearly, the summed line width of the LP plus the UP (84 cm^{-1}) is much smaller than the line width of the O−H stretch band outside the cavity. This difference arises because inhomogeneous broadening of the molecular peak does not contribute to the polariton line width—a phenomenon that was theoretically predicted decades ago[58] and has also been experimentally confirmed under VSC.[9]

Beyond the classical result, Figure 1b plots the quantum IR spectrum of liquid water outside (black line) or inside (red line) the cavity by Fourier transforming the Kubo-transformed quantum dipole autocorrelation function.[38,52] Outside the cavity, the O−H stretch band peaks near 3450 cm^{-1} and has a line width of γ_{OH} = 283 cm^{-1}. Compared to the classical result, this quantum peak is red-shifted by about 100 cm^{-1} and is also broadened, improving agreement with the experimental values[57] compared to the classical simulations. The red-shifting and broadening can be related to the inclusion of zero-point energy effects in TRPMD. Inside the cavity, when the cavity mode with frequency ω_c = 3450 cm^{-1} is resonantly coupled to the O−H stretch band with $\tilde{\varepsilon} = 4 \times 10^{-4}$ au, the Rabi splitting between the UP and LP (red line) is Ω_R = 720 cm^{-1}, in agreement with the classical result. The polariton line widths, however, become γ_{UP} = 65 cm^{-1} and γ_{LP} = 129 cm^{-1}. These values are significantly broadened compared with the classical results by roughly a factor of 2, whereas the line width of the quantum O−H band exceeds the classical result by only 30%.

Table 1 further summarizes the quantum and classical values of the Rabi splitting and polariton line widths. Clearly, the unchanged Rabi splitting shows that this quantity can be fully captured by classical mechanics. As far as the line shape is concerned, the polariton line shape seems to be more sensitive to the quantum treatment than the molecular line shape outside the cavity. Although one must always be aware of the limitations of TRPMD when simulating spectral line shapes,[49,59,60] namely that it may cause a broadening and loss of fine spectral features, the difference in the quantum and classical line widths for polaritons may also reflect a quantum effect (e.g., perhaps a faster quantum polariton relaxation rate than a classical one). Because polaritons are mostly harmonic under collective VSC,[61,a] TRPMD, a method that is expected to perform well in the harmonic limit, should describe polaritons more accurately than the anharmonic O−H stretch band. Future work is needed to investigate the origin of the polariton broadening.

Table 1. Simulated Quantities under VSC[a]

VSC quantity	classical	quantum
ω_c ($\approx\omega_0$) (cm^{-1})	3550	3400
Ω_R (cm^{-1})	715	720
γ_{UP} (cm^{-1})	24	65
γ_{LP} (cm^{-1})	60	129
ϵ_r	54.5 (54.4)	56.6 (59.0)

[a]These data were obtained from Figures 1 and 2, including the Rabi splitting (Ω_R), the LP or UP line width (γ_{LP} or γ_{UP}), and the static dielectric constant (ϵ_r) of liquid water. The ϵ_r values in parentheses are the corresponding outside-cavity results. For reference, the simulated O−H band line width is (classical) 215 cm^{-1} or (quantum) 283 cm^{-1}.

Next, we examine the static dielectric constant of liquid water under VSC. In general, by performing molecular dynamics simulations, the static dielectric constant (ϵ_r) of a molecular system can be obtained by using the following standard formula:[45]

$$\epsilon_r = 1 + \frac{4\pi\beta}{3V}(\langle \mathbf{d}^2 \rangle - \langle \mathbf{d} \rangle^2) \tag{2}$$

where V denotes the simulation cell volume and $\mathbf{d} = (d_{g,x}, d_{g,y}, d_{g,z})$ denotes the dipole moment vector of the molecular system in three dimensions. As a static equilibrium property, ϵ_r can be exactly evaluated by both PIMD and RPMD. However, to be consistent with the above IR results, we will perform TPRMD to obtain ϵ_r.

Figure 2a plots the calculated ϵ_r in the time domain for up to t = 20 ns both outside the cavity (black line) and under VSC (red line) for the classical simulations. Because the hydrogen-bonding network for liquid water restricts the relaxation of $\mathbf{d}$, in order for ϵ_r to converge, the simulation needs to run for more than 10 ns.[45,50,52] Figure 2b plots the analogous calculated ϵ_r inside and outside the cavity for the quantum simulations.

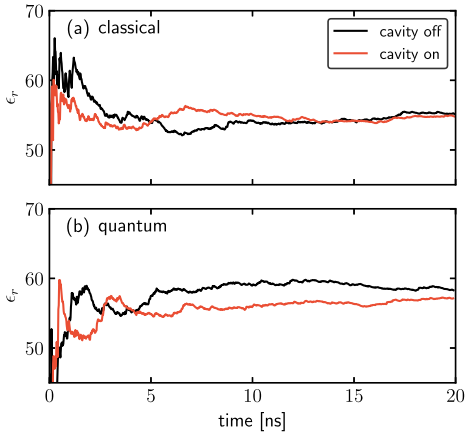

Figure 2. Static dielectric constant (ϵ_r) of liquid water as a function of time from (a) classical and (b) quantum simulations. The simulation parameters inside (red line) or outside (black line) the cavity are the same as Figure 1, except for a longer simulation time. Note that both quantum and classical simulations predict unchanged ϵ_r inside vs outside the cavity.

In Table 1 we report the values of ϵ_r by taking an average between t = 10 and 20 ns. Similar to our previous observation,[24,31] with a classical CavMD simulation, ϵ_r, a static equilibrium property, remains unchanged inside (ϵ_r = 54.5) vs outside (ϵ_r = 54.4) the cavity. For the quantum calculations,

https://doi.org/10.1021/acs.jpclett.2c00613
J. Phys. Chem. Lett. 2022, 13, 3890−3895

the result outside the cavity (ϵ_r = 59.0) agrees with a previous report.[52] Note that the values of ϵ_r inside (ϵ_r = 56.6) and outside (ϵ_r = 59.0) the cavity differ slightly, but this small difference is of the same order of magnitude as the fluctuations of ϵ_r for different simulations according to the literature.[52] Hence, we tentatively conclude that our quantum simulation does not predict a change in ϵ_r inside vs outside the cavity. Although the long-time static dielectric constant is similar inside and outside the cavity, the time-dependent dynamics, which reflects the change of molecular total dipole moment in the frequency domain, is quite different. This difference is consistent with the significant change in the IR spectrum inside vs outside the cavity, which also reflects the frequency-domain information about the total dipole moment.

Our observation that the simulated static dielectric constant does not change in a cavity is not consistent with a recent experiment[44] claiming that ϵ_r can be resonantly enhanced by nearly 50% under VSC and without external laser pumping. Such a discrepancy could arise for two different reasons. First, it may indicate that our simulation does not account for crucial experimental details needed for observing the reported phenomenon. For example, there could be hidden dynamical factors or nonequilibrium fluctuations in the actual experiment that cannot be modeled with our simple setup. This possibility is related to recent experimental efforts[20,21] that failed to reproduce some VSC catalytic experiments. In other words, within the framework of a single cavity mode plus a large collection of realistic molecules under thermal equilibrium, it might simply be impossible to obtain a resonant VSC effect. The second reason for the discrepancy could be that our current theoretical treatment may be incomplete even within the constraints of the model above. For example, we have included only 216 H_2O molecules coupled to a single cavity mode, whereas in VSC experiments the Fabry−Pérot cavities contain roughly $\sim 10^{10}$ molecules per mode volume and also a much more complicated cavity mode structure (i.e., the polaritonic dispersion relation)[8] than a single cavity mode. It might also be possible that a more pronounced cavity effect could emerge numerically if more accurate *ab initio* potentials were employed and/or the full cavity mode structure were simulated. In studies of ionic conductivity, the cavity could modify proton transfer, which in turn could influence the dielectric constant. Future work is needed to investigate these possibilities. Lastly, we note that the theory−experiment discrepancy is unlikely to stem from factors such as the electrolyte effect or cavity loss. In our simulations, a pure liquid water system is studied, whereas in experiments[44] a small amount of electrolyte is added to liquid water. Because the presence of the electrolyte does not significantly change the static dielectric constant of liquid water outside the cavity, however, it is unlikely that the experimentally observed cavity effect on the dielectric constant under VSC arises from the electrolyte effect. As far as cavity loss is concerned, unlike experiments[44] with a lossy cavity, our simulations do not include cavity loss. Although cavity loss can be important for IR spectra, including cavity loss is unlikely to modify equilibrium properties such as the static dielectric constant.

In summary, we have reported a quantum CavMD simulation of liquid water under VSC by TRPMD. Compared with the classical results, a quantum simulation predicts no change in the Rabi splitting but predicts broadening of the polariton line widths by roughly a factor of 2. This polaritonic broadening is more significant than the broadening of the O−H stretch band outside the cavity, and further study is needed to investigate its origin. Moreover, by combining path-integral techniques and CavMD, we have demonstrated a numerical approach for distinguishing between quantum and classical VSC effects. Although the current work does not show significant quantum effects, more intriguing VSC quantum effects might emerge when the following scenarios are studied: low-temperature dynamics, higher-order correlation functions, or nonlinear effects. These exciting directions may be investigated in the future.

■ ASSOCIATED CONTENT

Supporting Information

The Supporting Information is available free of charge at https://pubs.acs.org/doi/10.1021/acs.jpclett.2c00613.

Brief outline of the theory of PIMD and RPMD; brief introduction of CavMD; and the simulation details of this work (PDF)

■ AUTHOR INFORMATION

Corresponding Author

Tao E. Li − *Department of Chemistry, Yale University, New Haven, Connecticut 06520, United States;* orcid.org/0000-0003-0361-5687; Email: tao.li@yale.edu

Authors

Abraham Nitzan − *Department of Chemistry, University of Pennsylvania, Philadelphia, Pennsylvania 19104, United States; School of Chemistry, Tel Aviv University, Tel Aviv 69978, Israel;* orcid.org/0000-0002-8431-0967

Sharon Hammes-Schiffer − *Department of Chemistry, Yale University, New Haven, Connecticut 06520, United States;* orcid.org/0000-0002-3782-6995

Joseph E. Subotnik − *Department of Chemistry, University of Pennsylvania, Philadelphia, Pennsylvania 19104, United States*

Complete contact information is available at: https://pubs.acs.org/10.1021/acs.jpclett.2c00613

Notes

The authors declare no competing financial interest.

Code for reproducing this work is available at Github: https://github.com/TaoELi/cavity-md-ipi/.

■ ACKNOWLEDGMENTS

This material is based upon work supported by the U.S. National Science Foundation under Grant CHE1953701 (A.N.), US Department of Energy, Office of Science, Basic Energy Sciences, Chemical Sciences, Geosciences, and Biosciences Division under Award DE-SC0019397 (J.E.S.), and Air Force Office of Scientific Research under AFOSR Award FA9550-18-1-0134 (S.H.-S.). We thank Prof. Thomas E. Markland and Prof. Tomohiro Fukushima for insightful discussions.

■ ADDITIONAL NOTE

[a]One can understand the harmonic nature of polaritons by the following rationalization. When a polariton—a hybrid light−matter state—is in the second excited state, in the basis of individual molecules, the two polariton quanta can be represented by either (i) the second excited state of each individual anharmonic molecule or (ii) two different singly

excited molecules. When the number of molecules is large, the latter scenario dominates the representation. Hence, the anharmonic nature of each individual molecular vibrational spectrum will not cause anharmonicity to the polaritonic spectrum in the collective regime.

REFERENCES

(1) Ribeiro, R. F.; Martínez-Martínez, L. A.; Du, M.; Campos-Gonzalez-Angulo, J.; Yuen-Zhou, J. Polariton Chemistry: Controlling Molecular Dynamics with Optical Cavities. *Chem. Sci.* **2018**, *9*, 6325−6339.

(2) Flick, J.; Narang, P. Cavity-Correlated Electron-Nuclear Dynamics from First Principles. *Phys. Rev. Lett.* **2018**, *121*, 113002.

(3) Herrera, F.; Owrutsky, J. Molecular Polaritons for Controlling Chemistry with Quantum Optics. *J. Chem. Phys.* **2020**, *152*, 100902.

(4) Forn-Díaz, P.; Lamata, L.; Rico, E.; Kono, J.; Solano, E. Ultrastrong coupling regimes of light-matter interaction. *Rev. Mod. Phys.* **2019**, *91*, No. 025005.

(5) Frisk Kockum, A.; Miranowicz, A.; De Liberato, S.; Savasta, S.; Nori, F. Ultrastrong Coupling between Light and Matter. *Nat. Rev. Phys.* **2019**, *1*, 19−40.

(6) Xiang, B.; Xiong, W. Molecular Vibrational Polariton: Its Dynamics and Potentials in Novel Chemistry and Quantum Technology. *J. Chem. Phys.* **2021**, *155*, No. 050901.

(7) Garcia-Vidal, F. J.; Ciuti, C.; Ebbesen, T. W. Manipulating Matter by Strong Coupling to Vacuum Fields. *Science* **2021**, *373*, No. eabd0336.

(8) Li, T. E.; Cui, B.; Subotnik, J. E.; Nitzan, A. Molecular Polaritonics: Chemical Dynamics Under Strong Light−Matter Coupling. *Annu. Rev. Phys. Chem.* **2022**, *73*, 43.

(9) Long, J. P.; Simpkins, B. S. Coherent Coupling between a Molecular Vibration and Fabry−Perot Optical Cavity to Give Hybridized States in the Strong Coupling Limit. *ACS Photonics* **2015**, *2*, 130−136.

(10) George, J.; Shalabney, A.; Hutchison, J. A.; Genet, C.; Ebbesen, T. W. Liquid-Phase Vibrational Strong Coupling. *J. Phys. Chem. Lett.* **2015**, *6*, 1027−1031.

(11) Thomas, A.; George, J.; Shalabney, A.; Dryzhakov, M.; Varma, S. J.; Moran, J.; Chervy, T.; Zhong, X.; Devaux, E.; Genet, C.; et al. Ground-State Chemical Reactivity under Vibrational Coupling to the Vacuum Electromagnetic Field. *Angew. Chemie Int. Ed.* **2016**, *55*, 11462−11466.

(12) Thomas, A.; Lethuillier-Karl, L.; Nagarajan, K.; Vergauwe, R. M. A.; George, J.; Chervy, T.; Shalabney, A.; Devaux, E.; Genet, C.; Moran, J.; et al. Tilting a Ground-State Reactivity Landscape by Vibrational Strong Coupling. *Science* **2019**, *363*, 615−619.

(13) Lather, J.; Bhatt, P.; Thomas, A.; Ebbesen, T. W.; George, J. Cavity Catalysis by Cooperative Vibrational Strong Coupling of Reactant and Solvent Molecules. *Angew. Chemie Int. Ed.* **2019**, *58*, 10635−10638.

(14) Pang, Y.; Thomas, A.; Nagarajan, K.; Vergauwe, R. M. A.; Joseph, K.; Patrahau, B.; Wang, K.; Genet, C.; Ebbesen, T. W. On the Role of Symmetry in Vibrational Strong Coupling: The Case of ChargeTransfer Complexation. *Angew. Chemie Int. Ed.* **2020**, *59*, 10436−10440.

(15) Sau, A.; Nagarajan, K.; Patrahau, B.; Lethuillier-Karl, L.; Vergauwe, R. M. A.; Thomas, A.; Moran, J.; Genet, C.; Ebbesen, T. W. Modifying Woodward−Hoffmann Stereoselectivity Under Vibrational Strong Coupling. *Angew. Chem.* **2021**, *133*, 5776−5781.

(16) Lather, J.; George, J. Improving Enzyme Catalytic Efficiency by Co-operative Vibrational Strong Coupling of Water. *J. Phys. Chem. Lett.* **2021**, *12*, 379−384.

(17) Vergauwe, R. M. A.; Thomas, A.; Nagarajan, K.; Shalabney, A.; George, J.; Chervy, T.; Seidel, M.; Devaux, E.; Torbeev, V.; Ebbesen, T. W. Modification of Enzyme Activity by Vibrational Strong Coupling of Water. *Angew. Chemie Int. Ed.* **2019**, *58*, 15324−15328.

(18) Hirai, K.; Ishikawa, H.; Chervy, T.; Hutchison, J. A.; Uji-i, H. Selective Crystallization via Vibrational Strong Coupling. *Chem. Sci.* **2021**, *12*, 11986−11994.

(19) Joseph, K.; Kushida, S.; Smarsly, E.; Ihiawakrim, D.; Thomas, A.; ParaviciniBagliani, G. L.; Nagarajan, K.; Vergauwe, R.; Devaux, E.; Ersen, O.; et al. Supramolecular Assembly of Conjugated Polymers under Vibrational Strong Coupling. *Angew. Chemie Int. Ed.* **2021**, *60*, 19665−19670.

(20) Imperatore, M. V.; Asbury, J. B.; Giebink, N. C. Reproducibility of Cavity-Enhanced Chemical Reaction Rates in the Vibrational Strong Coupling Regime. *J. Chem. Phys.* **2021**, *154*, 191103.

(21) Wiesehan, G. D.; Xiong, W. Negligible Rate Enhancement from Reported Cooperative Vibrational Strong Coupling Catalysis. *J. Chem. Phys.* **2021**, *155*, 241103.

(22) Galego, J.; Climent, C.; Garcia-Vidal, F. J.; Feist, J. Cavity Casimir-Polder Forces and Their Effects in Ground-State Chemical Reactivity. *Phys. Rev. X* **2019**, *9*, No. 021057.

(23) Campos-Gonzalez-Angulo, J. A.; Ribeiro, R. F.; Yuen-Zhou, J. Resonant Catalysis of Thermally Activated Chemical Reactions with Vibrational Polaritons. *Nat. Commun.* **2019**, *10*, 4685.

(24) Li, T. E.; Nitzan, A.; Subotnik, J. E. On the Origin of Ground-State Vacuum-Field Catalysis: Equilibrium Consideration. *J. Chem. Phys.* **2020**, *152*, 234107.

(25) Campos-Gonzalez-Angulo, J. A.; Yuen-Zhou, J. Polaritonic Normal Modes in Transition State Theory. *J. Chem. Phys.* **2020**, *152*, 161101.

(26) Li, X.; Mandal, A.; Huo, P. Cavity Frequency-Dependent Theory for Vibrational Polariton Chemistry. *Nat. Commun.* **2021**, *12*, 1315.

(27) Sidler, D.; Schäfer, C.; Ruggenthaler, M.; Rubio, A. Polaritonic Chemistry: Collective Strong Coupling Implies Strong Local Modification of Chemical Properties. *J. Phys. Chem. Lett.* **2021**, *12*, 508−516.

(28) Du, M.; Campos-Gonzalez-Angulo, J. A.; Yuen-Zhou, J. Nonequilibrium Effects of Cavity Leakage and Vibrational Dissipation in Thermally Activated Polariton Chemistry. *J. Chem. Phys.* **2021**, *154*, No. 084108.

(29) Schäfer, C.; Flick, J.; Ronca, E.; Narang, P.; Rubio, A. Shining Light on the Microscopic Resonant Mechanism Responsible for Cavity-Mediated Chemical Reactivity. *arXiv* **2021**, 2104.12429.

(30) Triana, J. F.; Hernández, F. J.; Herrera, F. The Shape of the Electric Dipole Function Determines the Sub-picosecond Dynamics of Anharmonic Vibrational Polaritons. *J. Chem. Phys.* **2020**, *152*, 234111.

(31) Li, T. E.; Subotnik, J. E.; Nitzan, A. Cavity Molecular Dynamics Simulations of Liquid Water under Vibrational Ultrastrong Coupling. *Proc. Natl. Acad. Sci. U. S. A.* **2020**, *117*, 18324−18331.

(32) Li, T. E.; Nitzan, A.; Subotnik, J. E. Polariton Relaxation under Vibrational Strong Coupling: Comparing Cavity Molecular Dynamics Simulations against Fermi's Golden Rule Rate. *J. Chem. Phys.* **2022**, *156*, 134106.

(33) Li, T. E.; Nitzan, A.; Subotnik, J. E. Cavity Molecular Dynamics Simulations of Vibrational Polariton-enhanced Molecular Nonlinear Absorption. *J. Chem. Phys.* **2021**, *154*, No. 094124.

(34) Li, T. E.; Nitzan, A.; Subotnik, J. E. Collective Vibrational Strong Coupling Effects on Molecular Vibrational Relaxation and Energy Transfer: Numerical Insights via Cavity Molecular Dynamics Simulations**. *Angew. Chemie Int. Ed.* **2021**, *60*, 15533−15540.

(35) Li, T. E.; Nitzan, A.; Subotnik, J. E. Energy-Efficient Pathway for Selectively Exciting Solute Molecules to High Vibrational States via Solvent Vibration-Polariton Pumping. *arXiv* **2021**, 2104.15121.

(36) Parrinello, M.; Rahman, A. Study of an F Center in Molten KCl. *J. Chem. Phys.* **1984**, *80*, 860−867.

(37) Craig, I. R.; Manolopoulos, D. E. Quantum Statistics and Classical Mechanics: Real Time Correlation Functions from Ring Polymer Molecular Dynamics. *J. Chem. Phys.* **2004**, *121*, 3368−3373.

(38) Habershon, S.; Manolopoulos, D. E.; Markland, T. E.; Miller, T. F. Ring-Polymer Molecular Dynamics: Quantum Effects in

https://doi.org/10.1021/acs.jpclett.2c00613
J. Phys. Chem. Lett. 2022, 13, 3890−3895

Chemical Dynamics from Classical Trajectories in an Extended Phase Space. *Annu. Rev. Phys. Chem.* **2013**, *64*, 387−413.
(39) Markland, T. E.; Ceriotti, M. Nuclear Quantum Effects Enter the Mainstream. *Nat. Rev. Chem.* **2018**, *2*, No. 0109.
(40) Chowdhury, S. N.; Mandal, A.; Huo, P. Ring Polymer Quantization of the Photon Field in Polariton Chemistry. *J. Chem. Phys.* **2021**, *154*, No. 044109.
(41) Yang, P. Y.; Cao, J. Quantum Effects in Chemical Reactions under Polaritonic Vibrational Strong Coupling. *J. Phys. Chem. Lett.* **2021**, *12*, 9531−9538.
(42) Hiura, H.; Shalabney, A.; George, J. Cavity Catalysis — Accelerating Reactions under Vibrational Strong Coupling. *ChemRxiv* **2018**, DOI: 10.26434/chemrxiv.7234721.v4.
(43) Fukushima, T.; Yoshimitsu, S.; Murakoshi, K. Vibrational Coupling of Water from Weak to Ultrastrong Coupling Regime via Cavity Mode Tuning. *J. Phys. Chem. C* **2021**, *125*, 25832−25840.
(44) Fukushima, T.; Yoshimitsu, S.; Murakoshi, K. Inherent Promotion of Ionic Conductivity via Coherent Vibrational Strong Coupling of Water. *ChemRxiv* **2021**, DOI: 10.26434/CHEMRXIV-2021-ZK549.
(45) Paesani, F.; Zhang, W.; Case, D. A.; Cheatham, T. E.; Voth, G. A. An Accurate and Simple Quantum Model for Liquid Water. *J. Chem. Phys.* **2006**, *125*, 184507.
(46) Tuckerman, M. *Statistical Mechanics: Theory and Molecular Simulation*; Oxford University Press: New York, 2010.
(47) Habershon, S.; Manolopoulos, D. E. Zero Point Energy Leakage in Condensed Phase Dynamics: An Assessment of Quantum Simulation Methods for Liquid Water. *J. Chem. Phys.* **2009**, *131*, 244518.
(48) Habershon, S.; Fanourgakis, G. S.; Manolopoulos, D. E. Comparison of Path Integral Molecular Dynamics Methods for the Infrared Absorption Spectrum of Liquid Water. *J. Chem. Phys.* **2008**, *129*, No. 074501.
(49) Rossi, M.; Ceriotti, M.; Manolopoulos, D. E. How to Remove the Spurious Resonances from Ring Polymer Molecular Dynamics. *J. Chem. Phys.* **2014**, *140*, 234116.
(50) Ceriotti, M.; Parrinello, M.; Markland, T. E.; Manolopoulos, D. E. Efficient Stochastic Thermostatting of Path Integral Molecular Dynamics. *J. Chem. Phys.* **2010**, *133*, 124104.
(51) Flick, J.; Ruggenthaler, M.; Appel, H.; Rubio, A. Atoms and Molecules in Cavities, from Weak to Strong Coupling in Quantum-Electrodynamics (QED) Chemistry. *Proc. Natl. Acad. Sci. U. S. A.* **2017**, *114*, 3026−3034.
(52) Habershon, S.; Markland, T. E.; Manolopoulos, D. E. Competing Quantum Effects in the Dynamics of a Flexible Water Model. *J. Chem. Phys.* **2009**, *131*, No. 024501.
(53) Liu, H.; Wang, Y.; Bowman, J. M. Transferable ab Initio Dipole Moment for Water: Three Applications to Bulk Water. *J. Phys. Chem. B* **2016**, *120*, 1735−1742.
(54) Kapil, V.; Rossi, M.; Marsalek, O.; Petraglia, R.; Litman, Y.; Spura, T.; Cheng, B.; Cuzzocrea, A.; Meißner, R. H.; Wilkins, D. M.; et al. i-PI 2.0: A universal force engine for advanced molecular simulations. *Comput. Phys. Commun.* **2019**, *236*, 214−223.
(55) Plimpton, S. Fast Parallel Algorithms for Short-Range Molecular Dynamics. *J. Comput. Phys.* **1995**, *117*, 1−19.
(56) Li, T. E. Cavity Molecular Dynamics Simulations Tool Sets. https://github.com/TaoELi/cavity-md-ipi, 2020.
(57) Bertie, J. E.; Lan, Z. Infrared Intensities of Liquids XX: The Intensity of the OH Stretching Band of Liquid Water Revisited, and the Best Current Values of the Optical Constants of H_2O(l) at 25 °C between 15,000 and 1 cm^{-1}. *Appl. Spectrosc.* **1996**, *50*, 1047−1057.
(58) Houdré, R.; Stanley, R. P.; Ilegems, M. Vacuum-field Rabi Splitting in the Presence of Inhomogeneous Broadening: Resolution of a Homogeneous Linewidth in an Inhomogeneously Broadened System. *Phys. Rev. A* **1996**, *53*, 2711−2715.
(59) Benson, R. L.; Trenins, G.; Althorpe, S. C. Which Quantum Statistics−Classical Dynamics Method is best for Water? *Faraday Discuss.* **2020**, *221*, 350−366.
(60) Kryvohuz, M.; Cao, J. Quantum-Classical Correspondence in Response Theory. *Phys. Rev. Lett.* **2005**, *95*, 180405.
(61) Campos-Gonzalez-Angulo, J. A.; Yuen-Zhou, J. Generalization of the Tavis-Cummings Model for Multi-level Anharmonic Systems: Insights on the Second Excitation Manifold. *arXiv* **2022**, 2202.01433.

https://doi.org/10.1021/acs.jpclett.2c00613
J. Phys. Chem. Lett. 2022, 13, 3890−3895